O.V. Sukhova

Solubility of Cu, Ni, Mn in Boron-Rich Fe-B-C Alloys

The Oles' Honchar Dnipro National University, Dnipro, Ukraine, sukhovaya@ukr.net

In the present study, the microstructure development and mechanical properties of the cast boron-rich Fe–B–C alloys cooled at 10 and 10^3 K/s were investigated as functions of alloying elements additions. These alloys were prepared in the following compositional ranges: B (10 - 14 wt.%), C (0.1 - 1.2 wt.%), M (5 wt.%), where M – Cu, Ni or Mn, balance Fe. Structural properties were characterized by quantitative metallography, X-Ray diffraction, scanning electron microscopy, and energy dispersive spectroscopy. Mechanical properties of the structural constituents, such as microhardness and fracture toughness, were measured by a Vickers indenter. Copper becomes negligibly incorporated into the phases $Fe(B,C)$ and $Fe_2(B,C)$ of the Fe–B–C alloys, but solubility limit forces the remaining solute into the residual liquid. As a result, the globular Cu inclusions are seen in the structure. As compared with copper, nickel has higher solubility in the constituent phases, with preferential solubility observed in the $Fe_2(B,C)$ crystals, where Ni occupies Fe positions. Having limited solubility, nickel also forms secondary Ni_4B_3 phase at the $Fe_2(B,C)$ boundaries. Manganese was found to dissolve completely in the Fe–B–C alloys forming substitutional solid solutions preferentially with $Fe(B,C)$ dendrites. By entering into the iron borides structure, Mn and Ni improve their ductility but lower microhardness. The peculiarities in the structure formation and properties of the doped boron-rich Fe–B–C alloys were explained with electronic structure of the alloying elements considered.

Key words: iron borides, alloying elements, solubility, cooling rate, mechanical properties.

Received 25 January 2021; Accepted 25 February 2021.

Introduction

Boron-rich Fe–B–C alloys containing more than 10 wt. % B are among the few alloys to have been studied in terms of several of their physical properties, such as hardness, elevated temperature strength, and thermal stability [1-3]. Previous studies have also shown that Fe–B–C alloys have excellent wear, oxidation, and corrosion resistance [4-5]. Besides, these alloys are easily available and have the favorable cost. However, these properties can only be used for technological applications in the form of coatings [6-9] or reinforcement particles in metal matrix composites [10-11] to circumvent their intrinsic brittleness.

To apply the boron-rich Fe–B–C alloys as fillers of composites fabricated by infiltration, the contact interaction processes between the filler and the molten Cu–Ni–Mn binder should be studied [12, 13]. These processes may be accompanied by diffusion of binder constituent components, specifically Cu, Ni or Mn, into solid Fe–B–C filler. The performance characteristics may drastically deteriorate in case of negative influence of the diffusing elements on the structure and properties of structural constituents of the Fe–B–C alloys [14, 15].

There have been some reports regarding to the effect of Cu, Ni or Mn on the microstructure and properties of the Fe–B–C alloys [16-19]. However, their examined compositions have been limited up to 3 wt. % B [20-22]. Moreover, while the effect of the alloying elements has been studied, the effect of cooling rate on their solubility has not attracted as much attention [23-25].

So, a better understanding of the morphological modifications and properties of the Fe–B–C alloys with additional elements are necessary for practical applications. Research of the Fe–B–C alloys doped by Cu, Ni or Mn and clarification of their structure is particularly important for further development of the (Cu–Ni–Mn)-matrix composites reinforced with Fe–B–C fillers. Moreover, solubility of the alloying elements may

be influenced by changing cooling rate of the filler. Therefore, the solidification sequence and properties of the boron-rich Fe–B–C alloys were investigated as functions of additional Cu, Ni or Mn amounts and cooling rate during solidification.

I. Experimental procedure

The composition of boron-rich Fe–B–C alloys, determined by chemical and spectral analyses, was within the concentration range of 10.0 - 14.0 % B, 0.1 - 1.2 % C, 5.0 % M (where M – Cu, Ni, Mn), Fe – the remainder (in wt. %). The specimens were prepared by melting the constituent elements of high purity (99.99 %) in a Tamman furnace and solidified at cooling rates of 10 and 10^3 K/s.

For microstructural characterization, metallographic sections were observed by light metallographic microscope Neophot-32 and scanning electron microscope Jeol-2010 F (SEM) equipped with energy-dispersive spectrometer (EDS). Composition and lattice parameters of the phases in the investigated alloys as a function of composition were determined by X-ray

diffractometer HZG-4A with CuK_α radiation.

The Vickers microhardness (H_μ) was measured using device PMT-3 from at least 10 different indentations, and the fracture toughness (K_{IC}) was evaluated from the crack length initiated at the corners of the Vickers microindentation using an empirical equation proposed in [26].

II. Experimental results and discussion

The master Fe–B–C alloys exhibit peritectic structure: primary dendrites of Fe(B,C) monoboride are observed in the background of peritectically formed Fe_2B hemiboride alloyed with carbon [27]. The $Fe_2(B,C)$ and Fe(B,C) phases have no noticeable solubility for copper (Fig. 1) which is also confirmed by lattice parameters measurements (Table 1). As a result, globular copper inclusions appear in the structure (Fig. 1, a). Copper does not cause substantial change in the dendrite parameters of Fe(B,C) crystals, as shown in Table 2, but slightly influences the microhardness and the fracture toughness of the major structural constituents (Table 3).

a

b

c
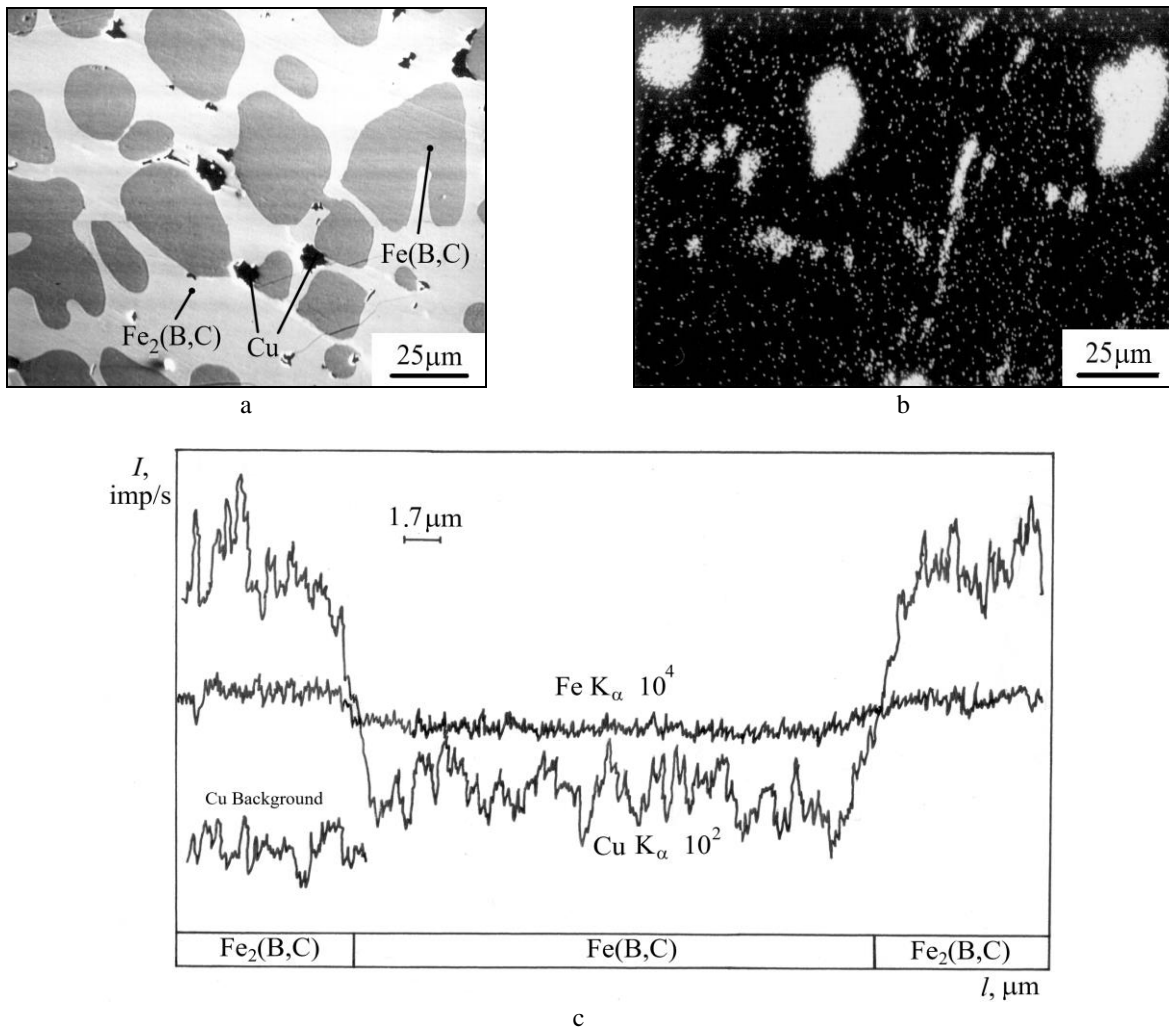
Fig. 1. SEM of polished cross-sections of Fe−12.1%B−0.12%C−5.0%Cu alloy: a – second electron image; b – elemental EDS X-ray mapping in CuK_α radiation; c – elemental profile along scanning line

Table 1

The lattice parameters of Fe(B,C) and Fe$_2$(B,C) crystals in the doped Fe–12.1B–0.1C–5.0M alloys cooled at 10 K/s

| Alloying element	Fe(B,C) (rhombic lattice)			Fe$_2$(B,C) (tetragonal lattice)		
	a, Å	b, Å	c, Å	a, Å	c, Å	c/a
–	5.5051 ± 0.0061	4.0628 ± 0.0097	2.9480 ± 0.0007	5.1130 ± 0.0008	4.2399 ± 0.0035	0.8292
Cu	5.5050 ± 0.0027	4.0590 ± 0.0036	2.9472 ± 0.0017	5.1131 ± 0.0004	4.2403 ± 0.0018	0.8293
Ni	5.5041 ± 0.0034	4.0627 ± 0.0026	2.9445 ± 0.0025	5.1116 ± 0.0041	4.2343 ± 0.0012	0.8284
Mn	5.5350 ± 0.0044	4.0651 ± 0.0032	2.9482 ± 0.0021	5.1154 ± 0.0024	4.2405 ± 0.0037	0.8290

Table 2

Influence of alloying elements on interdendritic distance (l_0, μm) and diameter of secondary dendritic arms (d_0, μm) of Fe(B,C) dendrites in the doped Fe–12.1B–0.1C–5.0M alloys

Alloying element	V_{cool} = 10 K/s		V_{cool} = 10^3 K/s	
	d_0	l_0	d_0	l_0
–	29.9 ± 0.9	33.1 ± 0.3	4.9 ± 0.2	5.2 ± 0.2
Cu	28.9 ± 0.8	32.2 ± 0.3	4.3 ± 0.1	4.6 ± 0.1
Ni	23.6 ± 0.3	29.0 ± 0.1	3.8 ± 0.1	4.1 ± 0.1
Mn	29.0 ± 0.7	31.3 ± 0.5	4.6 ± 0.2	4.8 ± 0.2

Nickel slightly dissolves in Fe$_2$(B,C) crystals, and only negligible content of this element is revealed in solid solution Fe(B,C) by EDS analysis (Fig. 2). This implies that, due to limited solubility, Ni is continually pushed out in the melt ahead of the moving solid-liquid interface into the interdendritic regions of growing Fe(B,C) dendrites slowing their growth and causing noticeable refinement (Table 2). As a result, the secondary crystals of Ni$_4$B$_3$ appear at the Fe$_2$(B,C) boundaries (Fig. 2, a).

a

b

c
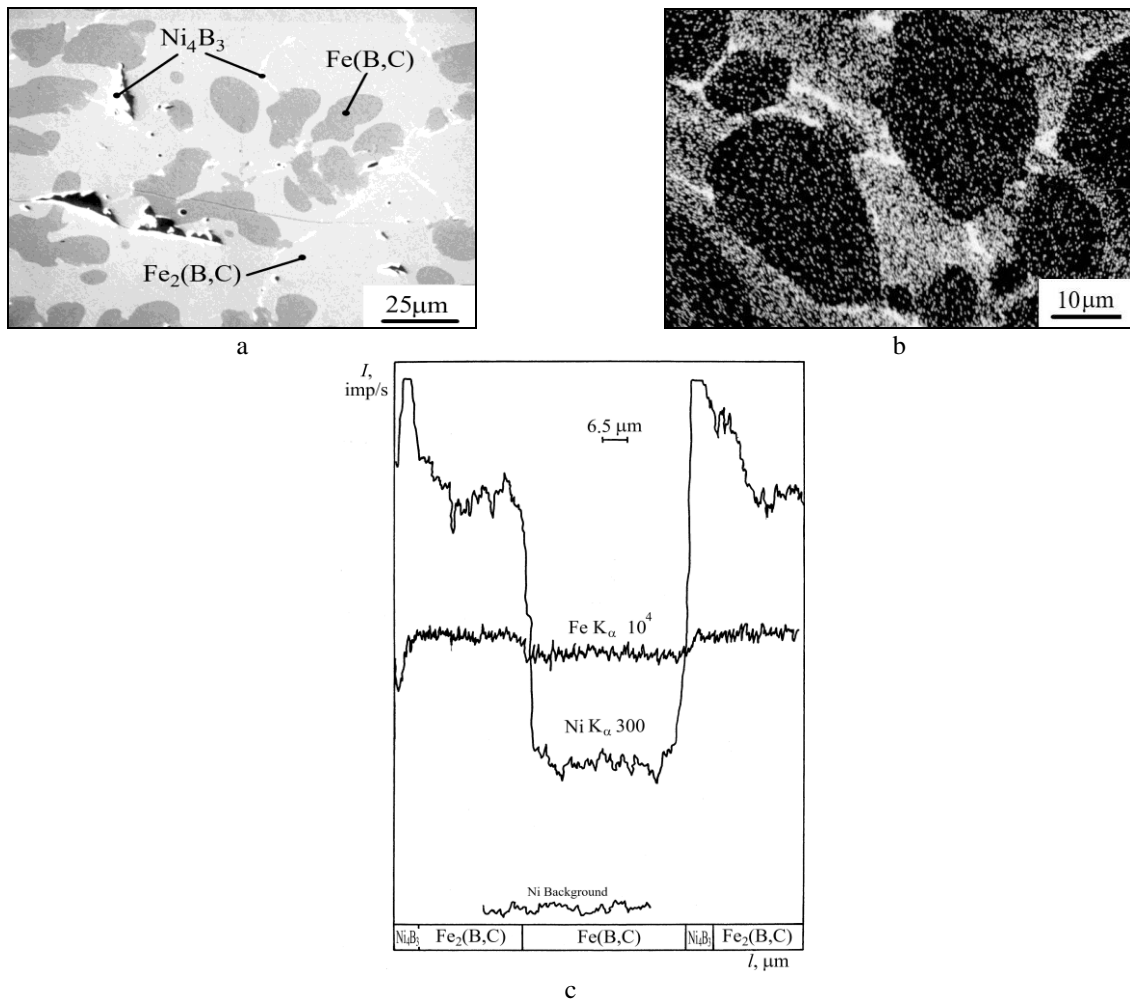
Fig. 2. SEM of polished cross-sections of Fe−12.1%B−0.12%C−5.0%Ni alloy: a – second electron image; b – elemental EDS X-ray mapping in NiK$_\alpha$ radiation; c – elemental profile along scanning line

Table 3

Influence of alloying elements on microhardness (H_μ, GPa) and fracture toughness (K_{1C}, MPa·$\sqrt{M}$) of Fe$_2$(B,C) and Fe(B,C) solid solutions in the doped Fe–12.1B–0.1C–5.0M alloys

Alloying element	V_{cool} = 10 K/s				V_{cool} = 10^3 K/s			
	Fe(B,C)		Fe$_2$(B,C)		Fe(B,C)		Fe$_2$(B,C)	
	H_μ	K_{1C}	H_μ	K_{1C}	H_μ	K_{1C}	H_μ	K_{1C}
−	17.8 ± 0.3	2.1 ± 0.2	15.8 ± 0.2	2.2 ± 0.3	20.1 ± 0.3	5.0 ± 0.2	17.0 ± 0.1	4.0 ± 0.1
Cu	17.7 ± 0.2	2.1 ± 0.1	15.6 ± 0.3	2.3 ± 0.2	20.1 ± 0.4	5.0 ± 0.1	16.8 ± 0.2	4.6 ± 0.3
Ni	17.1 ± 0.2	2.4 ± 0.1	15.3 ± 0.1	2.8 ± 0.2	19.8 ± 0.3	5.2 ± 0.2	16.0 ± 0.3	−
Mn	17.2 ± 0.1	3.5 ± 0.1	15.2 ± 0.1	2.6 ± 0.2	19.3 ± 0.2	−	15.9 ± 0.2	−

Manganese completely dissolves in the Fe–B–C alloys, as illustrated in Fig. 3. This element, that has some solubility in Fe$_2$(B,C) phase, is mainly accommodated in the structure of Fe(B,C) crystals. Manganese slightly decreases dendrite parameters of the doped Fe(B,C) crystals (Table 2).

Manganese like nickel occupies iron positions in the crystalline lattices of the constituent phases forming substitutional solid solutions as the results of XRD measurements show (Table 1). Besides, these elements decrease microhardness H_μ and enhance the fracture toughness K_{1C} of the constituent phases (Table 3).

With cooling rate increasing from 10 to 10^3 K/s, the structural composition of the boron-rich Fe–B–C alloys doped with Cu, Ni or Mn yields no significant changes, only constituent phases become smaller (Table 2). Solubility behaviour of the alloying elements proves to be similar to that in the alloys cooled at 10 K/s (Table 4). Their additions decrease microhardness H_μ and increase fracture toughness K_{1C} of Fe$_2$(B,C) and Fe(B,C) phases in the following sequence: Cu→Ni→Mn (Table 3).
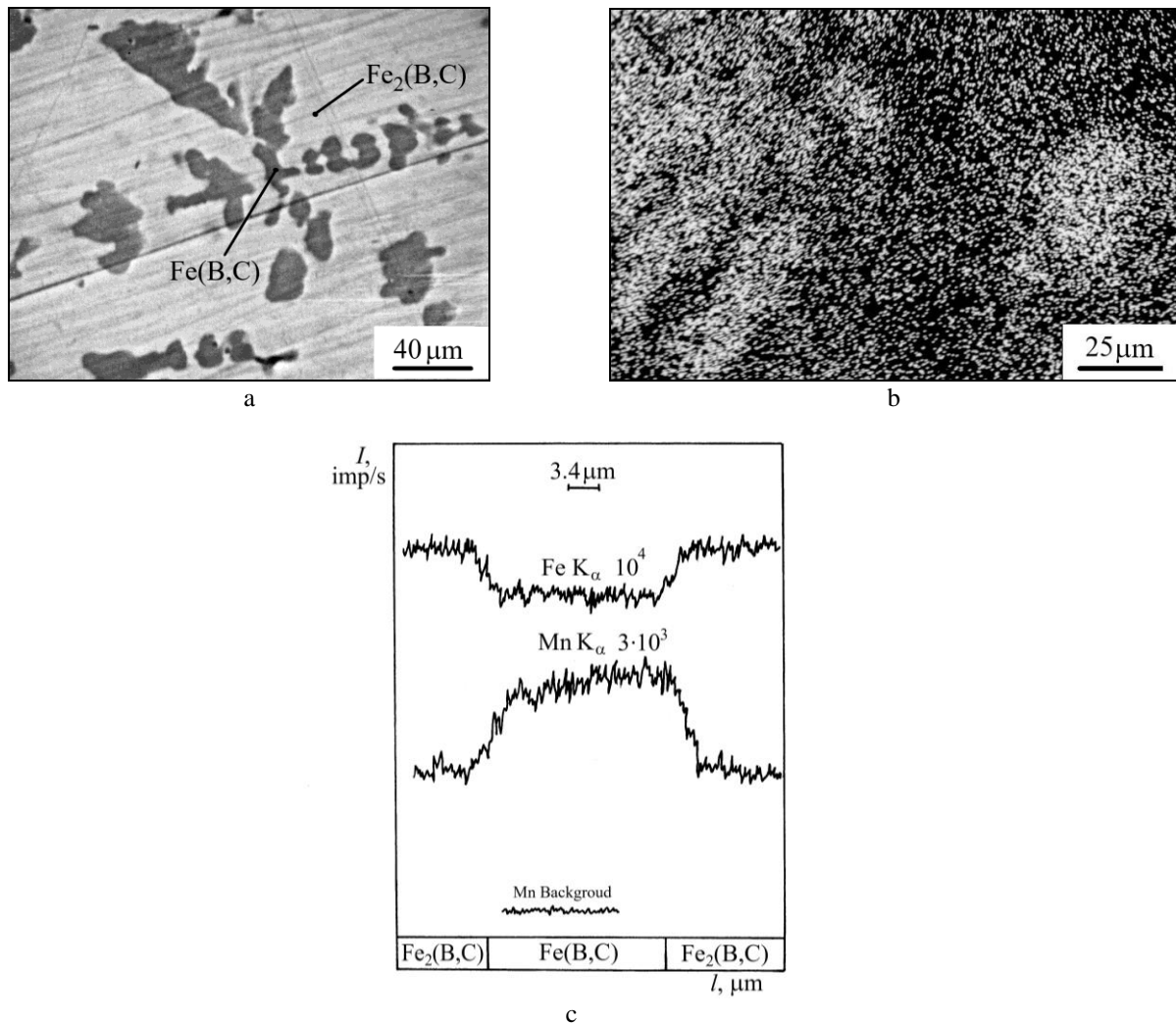

a

b

c

Fig. 3. SEM of polished cross-sections of Fe−12.1%B−0.12%C−5.0%Mn alloy: a – second electron image; b – elemental EDS X-ray mapping in MnK$_\alpha$ radiation; c – elemental profile along scanning line

Table 4

The lattice parameters of Fe(B,C) and Fe_2(B,C) crystals in the doped Fe–12.1B–0.1C–5.0M alloys
cooled at 10^3 K/s

Alloying element	Fe(B,C) (rhombic lattice)			Fe_2(B,C) (tetragonal lattice)		
	a, Å	b, Å	c, Å	a, Å	c, Å	c/a
–	5.5041 ± 0.0052	4.0596 ± 0.0106	2.9501 ± 0.0037	5.1120 ± 0.0001	4.2418 ± 0.0011	0.8298
Cu	5.5031 ± 0.0002	4.0590 ± 0.0022	2.9502 ± 0.0018	5.1123 ± 0.0012	4.2413 ± 0.0026	0.8296
Ni	5.5009 ± 0.0010	4.0588 ± 0.0008	2.9697 ± 0.0011	5.1100 ± 0.0004	4.2367 ± 0.0003	0.8291
Mn	5.5065 ± 0.0027	4.0640 ± 0.0033	2.9573 ± 0.0037	5.1144 ± 0.0024	4.2447 ± 0.0035	0.8299

The observed peculiarities in the solubility of Cu, Ni, and Mn in the structural constituents of the boron-rich Fe–B–C alloys may be explained as follows. Mn noticeably dissolves in the lattice of Fe(B,C) phase, but Ni – in the lattice of Fe_2(B,C) crystals. It may be assumed that, in the first place, the propensity for the solutes to form solid solutions involves the crystallographic aspect. The metallic radii of individual metal atoms increase in the following order: $Ni < Fe \leq Cu < Mn$ [28]. It makes understandable why Mn is predominantly dissolved in the rhombic lattice of Fe(B,C) than in more close-packed tetragonal lattice of Fe_2(B,C) and why Ni behaves opposite. The Mn and Ni solute atoms incorporate into the solvent crystalline lattices substitutionally by replacing iron atoms. Compared with manganese, nickel has smaller atomic radius and, therefore, affect the lattice parameters of the phases in a lower extent.

However, considering only the crystallographic aspect does not allow to explain why manganese, which atoms are larger than the iron atoms, has complete solubility but copper which atoms have similar size negligibly dissolves in the iron borides. Therefore, in addition to crystallographic aspect, the electronic structure of alloying elements should be considered. As known, the structure and properties of Fe_2(B,C) phase depend on the strength and directionality of the Fe–B and Fe–Fe bonds, and Fe(B,C) phase – on those of the B–B and Fe–Fe bonds [29]. The strength of these bonds is determined by the distraction of collectivized valence electrons of iron. The valence electrons of Mn are partially localized in the stable d^5-configurations and partially are collectivized. That is why, this element acts as electron acceptor. In electronic exchange between the atoms of iron and manganese, some electrons of iron localized in d^{10}-configurations transfer to d^5-configurations of manganese with energy gain. This contributes to the complete solubility of manganese in the lattices of iron borides.

As compared with manganese, nickel and copper have much lower electron localization degree that drastically decreases up to 2 % and 0 % correspondingly [30]. Therefore, acceptor ability of nickel used to be worse than that of manganese. As a result, this element has limited solubility in the iron borides. Electron configuration of copper is $d^{10}s^2$, therefore its ions cannot accept additional electrons and may be only donors of valence electrons. Any rearrangement of the bonding electrons in such system may result in the energetically non-advantageous destruction of the stable configurations. Therefore the solubility of Cu in Fe(B,C) or Fe_2(B,C) crystals is negligible.

Thus, the ions of alloying elements form to boron the same interatomic bonds as iron. As a result of the substitution of Fe by Mn or Ni the fewer bonding electrons take part in the electronic exchange. The B–B and Fe–B bonds become weaker and, therefore, the microhardness and the brittleness of the Mn- and Ni-containing solid solutions are found to decrease.

Conclusions

Substitution of Fe in boron-rich Fe–B–C alloys, containing 10.0 - 14.0 % B; 0.1 - 1.2 % C; Fe – the remainder, by 5.0 M (where M – Cu, Ni, or Mn) (in wt. %) does not greatly affect the solidification morphology of the Fe(B,C) and Fe_2(B,C) solid solutions that are major structural constituents of the alloys. The solidification process consists of the primary crystallization of Fe(B,C) dendrites and peritectic reaction forming the Fe_2(B,C) phase.

The negligible dissolution of Cu in the Fe–B–C alloys is responsible for the appearance of globular inclusions of copper in the structure. This result may be explained by electronic structure of copper that does not supply necessary electrons for the electronic exchange. Copper influences the mechanical properties of the Fe–B–C alloys via precipitation of secondary copper globules that may enhance, for example, antifriction properties of the alloys.

As compared with copper, solubility of nickel in the Fe–B–C alloys increases and prevails in Fe_2(B,C) phase. Nickel has a limited solubility and, therefore, this element is also found in the alloys in the form of Ni_4B_3 crystals precipitated at Fe_2(B,C) boundaries. Ni introduces the smallest lattice distortions which relates to the relatively small differences in the atomic sizes between the iron and substituting atom.

When adding manganese to Fe–B–C alloys, this element has complete solubility in the structural constituents, preferentially dissolving in Fe(B,C) phase. The higher solubility of manganese against nickel may be explained by the higher acceptor ability of the element.

The atoms of nickel and manganese form substitutional solutions in the crystal lattices of iron borides which weakens bonds in the solid solutions. Therefore, alloying with nickel and manganese decreases microhardness and increases fracture toughness of structural constituents.

With cooling rate of the boron-rich Fe–B–C alloys increasing from 10 to 10^3 K/s, solubility of Cu, Ni and Mn in Fe(B,C) and Fe$_2$(B,C) solid solutions remains unchanged. The size of structural constituents decreases but their microhardness and fracture toughness increases.

The obtained results clearly demonstrate the ways to control the processes of contact interaction between the Fe–B–C fillers and the Cu–Ni–Mn matrix during infiltration of macroheterogeneous composite coatings featuring high abrasive and gas-abrasive wear resistance at elevated temperatures.

Sukhova O.V. – Full Professor, Dr Sci Eng., Professor of Experimental Physics Chair.

[1] V. Homolova, L. Ciripova, A. Vyrostkova, Journal of Phase Equilibria and Diffusion 36(6), 599 (2015) (https://doi.org/10.1007/s11669-015-0424-0).

[2] Z.F. Huang, J.D. Xing, S.Q. Ma, Y.M. Gao, M. Zheng, L.Q. Sun, Key Engineering Materials 732, 59 (2017) (https://doi.org/10.4028/www.scientific.net/kem.732.59).

[3] A. Sudo, T. Nishi, N. Shirasu, M. Takano, M. Kurata, Journal of Nuclear Science and Technology 52(10), 1308 (2015) (https://doi.org/10.1080/00223131.2015.1016465).

[4] X. Ren, H. Fu, J. Xing, Y. Yang, S. Tang, Journal of Materials Research 32(16), 304 (2017) (https://doi.org/10.1557/jmr.2017.304).

[5] P. Sang, H. Fu, Y. Qu, C. Wang, Y. Lei, Materialwissenschaft Und Werkstofftechnik 46(9), 962 (2015) (https://doi.org/10.1002/mawe.201500397).

[6] I.M. Spyrydonova, O.V. Sukhova, G.V. Zinkovskij, Metallurgical and Mining Industry 4(4), 2 (2012).

[7] S.I. Ryabtsev, V.A. Polonskyy, O.V. Sukhova, Powder Metallurgy and Metal Ceramics 58(9-10), 567 (2020) (https://doi.org/10.1007/s11106-020-00111-2).

[8] O.V. Sukhova, V.A. Polonskyy, K.V. Ustinova, Materials Science 55(2), 285 (2019) (https://doi.org/10.1007/s11003-019-00302-2).

[9] O.V. Sukhova, Y.V. Syrovatko, Metallofizika i Noveishie Tekhnologii 41(9), 1171 (2019) (https://doi.org/10.15407/mfint.41.09.1171).

[10] Z. M. Rykavets, J. Bouquerel, J.-B. Vogt, Z. A. Duriagina, V. V. Kulyk, T. L. Tepla, L. I. Bohun, T. M. Kovbasyuk, Progress in Physics of Metals 20(4), 620 (2019) (https://doi.org/10.15407/ufm.20.04.620).

[11] O.P. Ostash, V.V. Kulyk, T.M. Lenkovskiy, Z.A. Duriagina, V.V. Vira, T.L. Tepla, Archives of Materials Science and Engineering 90(2), 49 (2018) (https://doi.org/10.5604/01.3001.0012.0662).

[12] I.M. Spiridonova, E.V. Sukhovaya, S.B. Pilyaeva, O.G. Bezrukavaya, Metallurgical and Mining Industry 3, 58 (2002).

[13] Z.A. Duriagina, M.R. Romanyshyn, V.V. Kulyk, T.M. Kovbasiuk, A.M. Trostianchyn, I.A. Lemishka, Journal of Achievements in Materials and Manufacturing Engineering 100(2), 49 (2020) (https://doi.org/10.5604/01.3001.0014.3344).

[14] I.M. Spiridonova, O.V. Sukhova, A.P. Vashchenko, Metallofizika i Noveishie Tekhnologii 21(2), 122 (1999).

[15] O.P. Ostash, V.H. Anofriev, I.M. Andreiko, L.A. Muradyan, V.V. Kulyk, Materials Science 48(6), 697 (2013) (https://doi.org/10.1007/s11003-013-9557-7).

[16] Yu.G. Chabak, V.I. Fedun, T.V. Pastukhova, V.I. Zurnadzhy, S.P. Berezhnyy, V.G. Efremenko, Problems of Atomic Science and Technology 110(4), 97 (2017).

[17] S. Egashira, T. Sekiya, T. Ueno, M. Fujii, Mechanical Engineering Journal 6(6), 19 (2019) (https://doi.org/10.1299/mej.19-00297).

[18] M.I. Pashechko, K. Dziedzic, M. Barszcz, Advances in Science and Technology Research Journal 10(31), 194 (2016) (https://doi.org/10.12913/22998624/64020).

[19] K. Lee, M. Choi, G. Lee, M. Kim, J. Kim, IEEE Transactions on Magnetics 1-4, (2018) (https://doi.org/10.1109/tmag.2018.2878292).

[20] L. Sidney, Alloy Steel: Property and Use (Scitus Academics LLC, Wilmington, 2016).

[21] O.V. Sukhova, K.V. Ustinova, Functional Materials 26(3), 495 (2019) (https://doi.org/10.15407/fm26.03.495).

[22] J. Miettinen, V.-V. Visuri, T. Fabritius, Archives of Metallurgy and Materials 66(1), 297 (2021) (https://doi.org/10.24425/amm.2021.134787).

[23] W. Shenglin, China Welding 27 (4), 46 (2018) (https://doi.org/10.12073/j.cw.20180603001).

[24] M. Zhang, X. Wang, S. Liu, K. Qu, Journal of Rare Earths 13(5), (2019) (https://doi.org/10.1016/j.jre.2019.05.013).

[25] Z. Chen, S. Miao, L. Kong, X. Wei, F. Zhang, H. Yu, Materials 13(4), 975 (2020) (https://doi.org/0.3390/ma13040975).

[26] K. Niihara, R. Morena, P.H. Hasselman, Journal of Materials Science Letters 1, 13 (1982) (https://doi.org/10.1007/BF00724706).

[27] O.V. Sukhova, Physics and Chemistry of Solid State 21(2), 355 (2020) (https://doi.org/10.15330/pcss.21.2.355-360).

[28] C.J. Smithells, Metals Reference Book (Butterworth and Co., London & Boston, 1976).

[29] G. Li, D. Wang, Journal of Physics of Condensed Matter 1, 1799 (1989).

[30] G.V. Samsonov, I.F. Pryadko, L.F. Pryadko, Electron Localization in Solids (Nauka, Moscow, 1976).

O.V. Sukhova

О.В. Сухова

Розчинність Cu, Ni, Mn у високобористих сплавах Fe-B-C

Дніпровський національний університет імені Олеся Гончара, Дніпро, Україна, sukhovaya@ukr.net

В роботі досліджували вплив легуючих елементів на процеси формування структури та механічні властивості литих високобористих сплавів Fe–B–C, охолоджених зі швидкостями 10 і 10^3 К/с. Склад сплавів знаходився в наступному концентраційному діапазоні: В (10 - 14 ваг.%), С (0,1 - 1,2 ваг.%), М (5 ваг.%), де М – Cu, Ni чи Mn, Fe – залишок. Структуру сплавів вивчали методами кількісної металографії, рентгеноструктурного аналізу, сканувальної електронної мікроскопії, рентгеноспектрального мікроаналізу. Механічні властивості структурних складових, а саме мікротвердість і коефіцієнт тріщиностійкості, вимірювали на мікротвердомірі Віккерса. Мідь має нехтовно малу розчинність у фазах Fe(B,C) та $Fe_2(B,C)$ високобористих сплавів Fe–B–C, тому цей елемент залишається в рідині під час кристалізації. В результаті по її закінченні в структурі спостерігаються глобулярні включення Cu. Порівняно з міддю нікель розчиняється в структурних складових сплавів у більшій кількості, переважно заміщуючи Fe в решітці фази $Fe_2(B,C)$. Маючи обмежену розчинність, нікель також утворює вторинну фазу Ni_4B_3 по границях кристалів $Fe_2(B,C)$. Марганець повністю розчиняється в структурних складових сплавів Fe–B–C, заміщуючи залізо переважно в кристалічній ґратці фази Fe(B,C). Потрапляючи в структуру боридів заліза, Mn і Ni підвищують їх пластичність, але знижують мікротвердість. Особливості структуроутворення та властивості легованих високобористих сплавів Fe–B–C пояснено з урахуванням електронної структури легуючих елементів.

Ключові слова: бориди заліза, легуючі елементи, розчинність, швидкість охолодження, механічні властивості.